

# Spatial Prediction of Undersampled Electromagnetic Fields

D. V. S. S. N. Karteekya Sastry, Chandan Bhat, and Uday K. Khankhoje

Department of Electrical Engineering, Indian Institute of Technology Madras, India

**Abstract**— We present a method to accurately predict the electromagnetic fields in an indoor setting using a limited number of measurements of scattered electromagnetic fields. We consider a room with a single object inside and a transmitter at the center of the room, and generate synthetic measurements using a Boundary Integral (BI) solver. We use Huygens’ principle to set up a linear relation between the measured fields and the tangential electric and magnetic fields on the scatterers’ surfaces — the latter being the unknowns that we seek to estimate. Since we want to use as few measurements as possible, the above relation is ill-posed and we regularize the solution by means of seeking a minimum L1-norm solution. The tangential fields are represented in various bases (Fourier series, Wavelet and Discrete Cosine Transform (DCT)) to determine the basis which results in the most sparse representation of the solution. Once the tangential fields are obtained, we use Huygens’ principle once again to obtain the field everywhere in the domain and compare it with the true solution. We present a study of the variation in error with increasing observations, increasing number of basis functions and different types of basis functions. We also present a study of the sparsity of the solution in different bases.

## 1. INTRODUCTION

Prediction of spatial electromagnetic fields, given a few measurements is of great importance in a number of situations, most notably indoor positioning systems [1, 2] and WiFi access point positioning [3] in various environments. In this paper, we present a novel method for the spatial prediction of electromagnetic fields from a few measurements. The problem we aim to solve is as follows:

*Consider a room with an antenna (e.g., a WiFi router) and a few objects inside. Can we determine the field everywhere inside the room?*

A trivial way to accomplish this task is to manually measure the field everywhere. However, this is quite tedious and time consuming. Instead we try to accomplish this task using only a few measurements. This is done by representing the field measured at each location as a linear combination of the tangential fields on the scatterers (the wall and the scattering object) using Huygens principle. This linear system of equations (which is under-determined as we want to reconstruct the field with as few measurements as possible) is then solved for the tangential fields. The tangential fields are in turn used to find the field everywhere in the room.

The set of basis in which the tangential fields are expanded is of considerable importance. Certain choices of bases admit a more sparse solution for the system. By compressive sensing principles, a sparse signal can be recovered from far fewer samples than a relatively dense signal [4]. We test for sparsity in Fourier series basis, wavelet basis and DCT basis. This paper is an extension of our earlier work [5].

This paper is organized as follows: Section 2 contains the theoretical details of the formulation. Section 3 explains the setup of the simulation and presents the numerical results. Finally, we present a discussion of the earlier presented results in Section 4.

## 2. THEORY

Consider the schematic in Figure 1 which shows a two dimensional (2D) computational domain which is illuminated using a transverse magnetic polarization. At any point in Region 1, we can express the  $z$ -component of the electric field,  $\phi(r)$ , using Huygens’ principle [6, 7] as:

$$\begin{aligned} \phi(r) = & \phi_{in}(r) - \oint_{S_w} [g(r, r') \nabla' \phi_w(r') - \phi_w(r') \nabla' g(r, r')] \cdot \hat{n}_w dr' \\ & - \oint_{S_o} [g(r, r') \nabla' \phi_o(r') - \phi_o(r') \nabla' g(r, r')] \cdot \hat{n}_o dr', \end{aligned} \quad (1)$$

where  $\phi_{in}(r)$  is the incident electric field,  $g(r, r') = (j/4)H_0^{(2)}(k_0|r-r'(x)|)$  is the Green’s function in Region 1,  $S_w$  is the inner surface of the enclosing wall and  $S_o$  is the contour enclosing the scatterer,

and primed coordinates correspond to points on either of these contours. It is important to note that the permittivity of the object does not feature in these equations and that it is sufficient for  $S_o$  to enclose this object. To arrive at a system of equations, we express the unknowns  $\phi_w$ ,  $\phi_o$ ,  $\nabla\phi_w$  and  $\nabla\phi_o$  in an appropriate basis, which can then be solved for the corresponding basis coefficients.

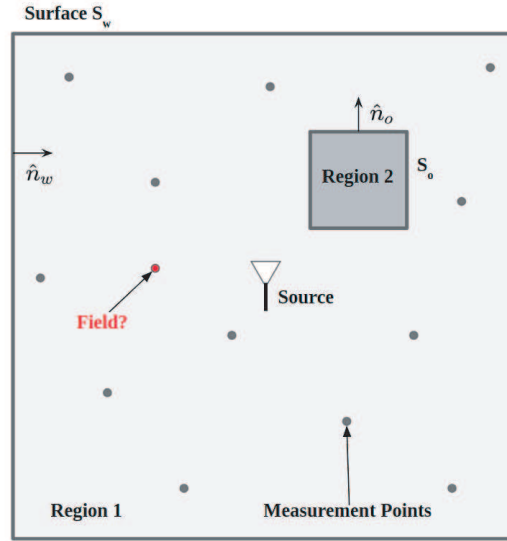


Figure 1: Schematic of spatial field prediction.

### 2.1. Fourier Series Basis

An  $L$ -periodic function  $f(x)$  can be expanded in an  $(N + 1)$  term Fourier series basis as:

$$f(x) = \sum_{n=-N/2}^{N/2} p_n e^{-j2\pi nx/L}, \quad 0 \leq x \leq L \quad (2)$$

where  $x$  represents the distance along the contour, and  $p_n$  is the coefficient basis.

We express the tangential fields on the surfaces  $S_w$  and  $S_o$  as a  $N_w$  and  $N_o$  term Fourier series (using Equation (2)) respectively. The Fourier series coefficients of  $\phi_w$ ,  $\nabla\phi_w$ ,  $\phi_o$  and  $\nabla\phi_o$  are  $a_n$ ,  $b_n$ ,  $c_n$  and  $d_n$  respectively. Substituting the expressions for the Fourier series expansions of the tangential fields in Equation (1),

$$\begin{aligned} \phi(r) - \phi_{in}(r) = & \sum_{n=-N_w/2}^{N_w/2} \oint_{S_w} \left( a_n \left( \zeta^{nx} \frac{jk_0}{4\rho_r} H_1^{(2)}(k_0\rho_r)(\vec{r}_v) \cdot \hat{n}_w \right) - b_n \left( \zeta^{nx} \frac{j}{4} H_0^{(2)}(k_0\rho_r) \right) \right) dx \\ & + \sum_{n=-N_o/2}^{N_o/2} \oint_{S_o} \left( c_n \left( \xi^{nx} \frac{jk_0}{4\rho_r} H_1^{(2)}(k_0\rho_r)(\vec{r}_v) \cdot \hat{n}_o \right) - d_n \left( \xi^{nx} \frac{j}{4} H_0^{(2)}(k_0\rho_r) \right) \right) dx, \quad (3) \end{aligned}$$

where  $\zeta = e^{-j2\pi/L_w}$ ,  $\xi = e^{-j2\pi/L_o}$ ,  $\rho_r = |r - r'(x)|$ , and  $r_v = r - r'(x)$ . Observe that the geometry of the problem is encoded in the coefficients of the above equation. The field  $\phi(r) - \phi_{in}(r)$  is measured at locations  $r_1, r_2, \dots, r_{2m}$ . Let

$$\begin{aligned} A_{mk} &= \oint_{S_w} \zeta^{nx} \frac{jk_0}{4\rho_{r_m}} H_1^{(2)}(k_0\rho_{r_m})(\vec{r}_v) \cdot \hat{n} dx & B_{mk} &= - \oint_{S_w} \zeta^{nx} \frac{j}{4} H_0^{(2)}(k_0\rho_{r_m}) dx \\ C_{mk} &= \oint_{S_o} \xi^{nx} \frac{jk_0}{4\rho_{r_m}} H_1^{(2)}(k_0\rho_{r_m})(\vec{r}_v) \cdot \hat{n} dx & D_{mk} &= - \oint_{S_o} \xi^{nx} \frac{j}{4} H_0^{(2)}(k_0\rho_{r_m}) dx \end{aligned}$$

Now assume that we have  $l$  measurements of the field, and  $N = 2(N_w + N_o)$  unknowns. This will result in a linear system of equations  $\mathcal{A}x = b$  where  $\mathcal{A}$  is a matrix of dimension  $l \times N$ ,  $x$  is a  $N \times 1$

vector of the  $N$  unknowns and  $b$  is  $l \times 1$  vector containing the  $l$  measurements. This linear system is then solved to get the Fourier coefficients of the tangential fields on the surfaces.

$$\begin{aligned}
 & \begin{bmatrix} A_{11} & \dots & A_{1N_o} & B_{11} & \dots & B_{1N_w} & C_{11} & \dots & C_{1N_w} & D_{11} & \dots & D_{1N_w} \\ A_{21} & \ddots & A_{2N_o} & B_{21} & \ddots & B_{2N_w} & C_{21} & \ddots & C_{2N_w} & D_{21} & \ddots & D_{2N_w} \\ \vdots & \dots & \vdots & \vdots & \dots & \vdots & \vdots & \dots & \vdots & \vdots & \dots & \vdots \\ A_{l1} & \dots & A_{lN_o} & B_{l1} & \dots & B_{lN_w} & C_{l1} & \dots & C_{lN_w} & D_{l1} & \dots & D_{lN_w} \end{bmatrix} \begin{bmatrix} a_1 \\ \vdots \\ a_{N_o} \\ b_1 \\ \vdots \\ b_{N_o} \\ c_1 \\ \vdots \\ c_{N_w} \\ d_1 \\ \vdots \\ d_{N_w} \end{bmatrix} \\
 & = \begin{bmatrix} \phi_s(r_1) \\ \phi_s(r_2) \\ \vdots \\ \phi_s(r_l) \end{bmatrix},
 \end{aligned}$$

where  $\phi_s(r_i)$  is the scattered field at location  $r_i$ . Once the Fourier series coefficients are determined, the tangential fields can be calculated using Equation (2). Huygens' principle can then be used to calculate the electromagnetic fields everywhere in Region 1.

## 2.2. Wavelet Basis

Next, we consider the Wavelet basis. In order to conveniently express the unknowns, we first write the system equation in pulse basis (given below):

$$f_i(x) = \begin{cases} 1 & r_{i-1} \leq x \leq r_i \\ 0 & \text{else} \end{cases}$$

Using this basis, we get the following matrix coefficients

$$\begin{aligned}
 A_{mk} &= \int_{r_{w,k-1}}^{r_{w,k}} \frac{jk_0}{4\rho_{r_m}} H_1^{(2)}(k_0\rho_{r_m})(\vec{r}_v) \cdot \hat{n} dx & B_{mk} &= - \int_{r_{w,k-1}}^{r_{w,k}} \frac{j}{4} H_0^{(2)}(k_0\rho_{r_m}) dx \\
 C_{mk} &= \int_{r_{o,k-1}}^{r_{o,k}} \frac{jk_0}{4\rho_{r_m}} H_1^{(2)}(k_0\rho_{r_m})(\vec{r}_v) \cdot \hat{n} dx & D_{mk} &= - \int_{r_{o,k-1}}^{r_{o,k}} \frac{j}{4} H_0^{(2)}(k_0\rho_{r_m}) dx
 \end{aligned}$$

where  $r_w$  denotes the discretized points on the wall and  $r_o$  denotes the discretized points on the object. Let the matrix populated using this basis be  $\mathcal{A}_p$ ; the system of equations in pulse basis is  $\mathcal{A}_p x = b$  where  $b$  is the set of measurements and  $x$  represents the coefficients of the unknown tangential fields in the pulse basis; the latter is obtained as a concatenation of four column vectors  $x_1, x_2, x_3$  and  $x_4$  which correspond to  $\phi_w, \nabla\phi_w, \phi_o$  and  $\nabla\phi_o$ , respectively. Let  $W_1$  and  $W_2$  denote wavelet matrices of appropriate size such that  $\alpha_1 = W_1 x_1, \alpha_2 = W_1 x_2, \alpha_3 = W_2 x_3, \alpha_4 = W_2 x_4$  denote the wavelet coefficients of  $\phi_w, \nabla\phi_w, \phi_o$  and  $\nabla\phi_o$ , respectively. Let  $\alpha$  be a column vector such that  $\alpha = [\alpha_1, \alpha_2, \alpha_3, \alpha_4]^T$  and  $W$  be the following block diagonal matrix

$$W = \begin{bmatrix} W_1 & 0 & 0 & 0 \\ 0 & W_1 & 0 & 0 \\ 0 & 0 & W_2 & 0 \\ 0 & 0 & 0 & W_2 \end{bmatrix}$$

We can see that  $\alpha = Wx$  which implies,  $x = W^\dagger \alpha$  where  $W^\dagger$  is the pseudoinverse of  $W$ . Finally, we can rewrite the equation  $\mathcal{A}_p x = b$  in wavelet basis as

$$\mathcal{A}_p W^\dagger \alpha = b \quad (4)$$

This system of equation is solved for  $\alpha$ , and in the simplest approach, we can get back  $x$  from  $\alpha$  simply by using the relation  $x = W^\dagger \alpha$ .

### 2.3. Discrete Cosine Transform (DCT) Basis

Following the same method used for wavelet basis, we use the DCT matrices of the appropriate size,  $D_1$  and  $D_2$ , instead of using  $W_1$  and  $W_2$ . We then define a block diagonal matrix  $D$  in a similar way as the matrix  $W$ . Therefore, we have

$$\mathcal{A}_p D^{-1} \beta = b \quad (5)$$

where  $\beta$  represents the DCT coefficients. We can get back  $x$  from  $\beta$  simply by using the relation  $x = D^{-1} \beta$ .

### 2.4. Motivation for Compressive Sensing Approach

Compressive Sensing principles state that a sparse signal can be recovered from undersampled linear measurements provided certain conditions on the sensing matrix are obeyed [4]. These conditions are related to the restrictive isometry property, which are hard to verify in practice. Instead, we use the compressive sensing principle in our case heuristically. We would like to find out the set of basis which would result in a sparse solution for the system described here. This requires us to solve either of the following optimization problems depending on the choice of basis:

$$\begin{aligned} & \text{minimize } \|\gamma\|_1 \\ & \text{subject to } \|C\gamma - b\|_2^2 \leq \epsilon \end{aligned}$$

where  $\gamma = \alpha$  and  $C = \mathcal{A}_p W^\dagger$  for wavelet basis and  $\gamma = \beta$  and  $C = \mathcal{A}_p D^{-1}$  for wavelet basis.  $\epsilon$  is a positive constants of the order of the noise floor of the measurements.

## 3. NUMERICAL RESULTS

In this Section we present numerical results for the prediction of spatial electromagnetic fields using the formulations introduced in the previous Section. First, we explain the simulation setup and the method used to generate the synthetic measurements (corresponding to the schematic given in Figure 1). Then, we present the reconstructed tangential fields, reconstructed 2D fields and the corresponding errors in the reconstruction. All simulations are carried out in MATLAB 2018b on a computer with Intel Core i7-7700 CPU at 3.60 GHz and 16 GB RAM.

### 3.1. Simulation Setup

The object and the wall have a relative permittivity of  $\epsilon_r = 3.7 - 2.1j$ . The wall has dimensions  $6\lambda \times 6\lambda$  and object dimensions are  $\lambda \times \lambda$  where  $\lambda$  is the wavelength. We generate the ‘true’ tangential fields using a Boundary Integral solver, using pulse basis with a fine discretization of  $\lambda/40$ . Unless stated otherwise, we select  $l = 150$  locations randomly inside the simulation domain and outside the object (Region 1 in Figure 1) and obtain the ‘true’ electric fields at these points using Huygens principle. These values are then corrupted with Additive White Gaussian Noise (AWGN) of SNR 25 dB.

### 3.2. Field Prediction Results

To set-up the field prediction experiments, we consider 150 measurements and investigate the different basis functions discussed above.

#### *Fourier Series Basis*

Figures 2 and 3 show the estimated magnitudes of Fourier series coefficients and tangential fields from 150 measurements, using 60 basis functions on the objects and 80 on the wall which makes the total number of unknowns  $2(N_w + N_o) = 2(60 + 80) = 280$ .

#### *Wavelet and DCT Basis*

In generating the pulse basis matrix for estimation in wavelet and DCT basis, we use a discretization of  $\lambda/5$  on the scatter surface, which has been heuristically determined to give acceptable results without a high computational burden. Figures 4 and 5 show the estimated magnitudes of db2 wavelet coefficients and the corresponding tangential fields respectively for 150 measurements.

For estimation with the DCT basis, it has been found that performing a variant of L1 minimization, the so called ‘reweighted’ L1 minimization [8] algorithm gives good results. Figures 6 and 7 show the estimated magnitudes of the DCT coefficients and the corresponding tangential fields, respectively for 150 measurements.

Figure 8 contains the ‘true’ 2D field and the reconstructed 2D field using the previously calculated tangential fields. The 2D grid of points being considered has been discretized at a distance

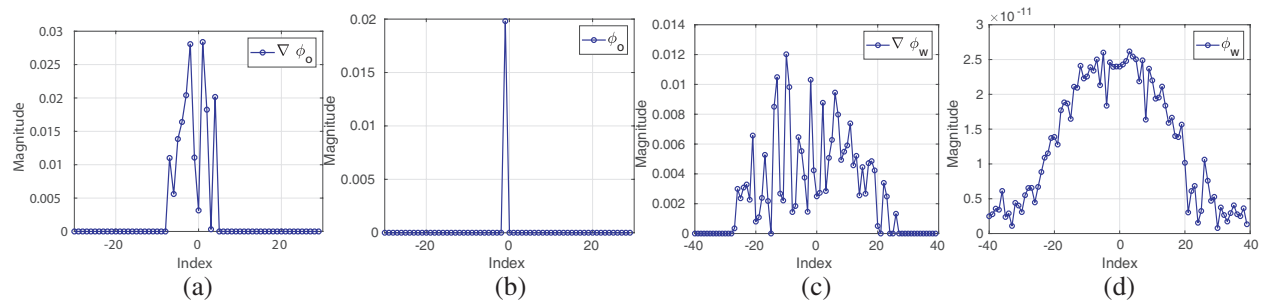


Figure 2: Magnitude of Fourier series coefficients of estimated tangential fields for 150 measurements. Coefficients corresponding to  $\phi_w$  are almost zero. There are 65 non zero coefficients. (a)  $\nabla\phi_o$ . (b)  $\phi_o$ . (c)  $\nabla\phi_w$ . (d)  $\phi_w$ .

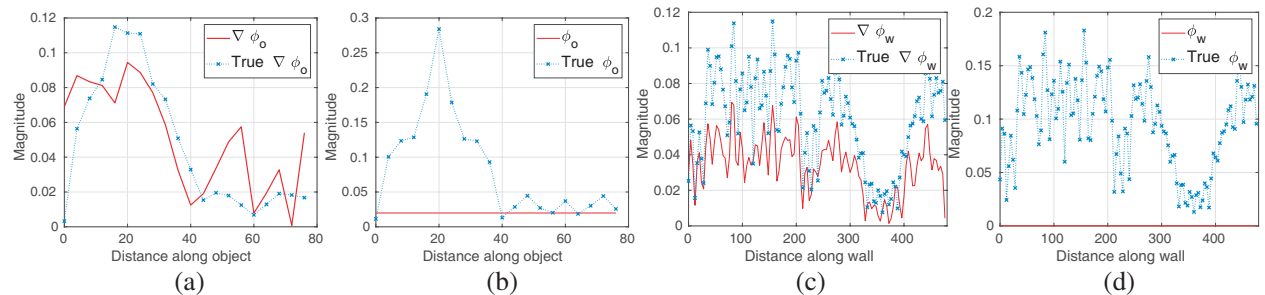


Figure 3: Magnitude of estimated tangential fields using Fourier series basis for 150 measurements.  $\phi_w$  is almost zero. (a)  $\nabla\phi_o$ . (b)  $\phi_o$ . (c)  $\nabla\phi_w$ . (d)  $\phi_w$ .

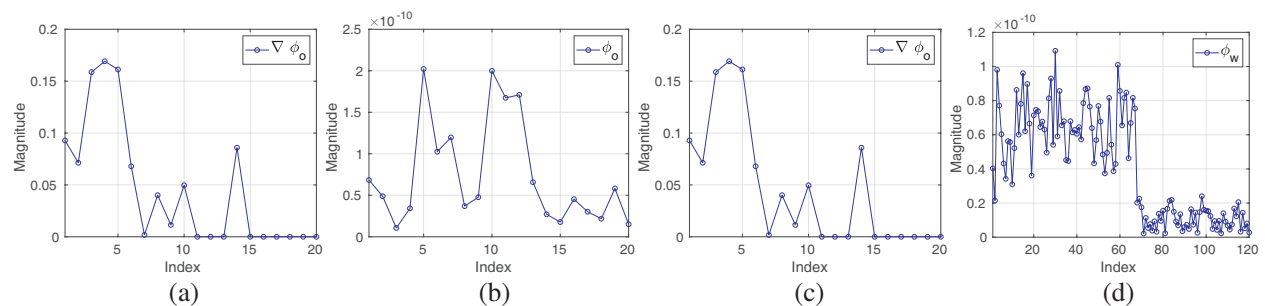


Figure 4: Magnitude of db2 wavelet coefficients of estimated tangential fields for 150 measurements. Coefficients corresponding to  $\phi_o$  and  $\phi_w$  are almost zero. There are 70 non zero coefficients. (a)  $\nabla\phi_o$ . (b)  $\phi_o$ . (c)  $\nabla\phi_w$ . (d)  $\phi_w$ .

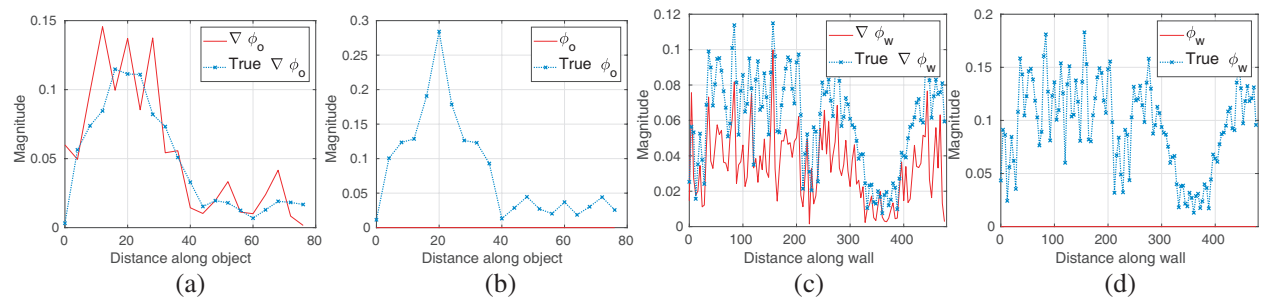


Figure 5: Magnitude of estimated tangential fields using db2 wavelet basis for 150 measurements.  $\phi_o$  and  $\phi_w$  is almost zero. (a)  $\nabla\phi_o$ . (b)  $\phi_o$ . (c)  $\nabla\phi_w$ . (d)  $\phi_w$ .

of  $\lambda/10$ . The error in reconstruction is calculated over this 2D grid using the ‘true’ 2D field as

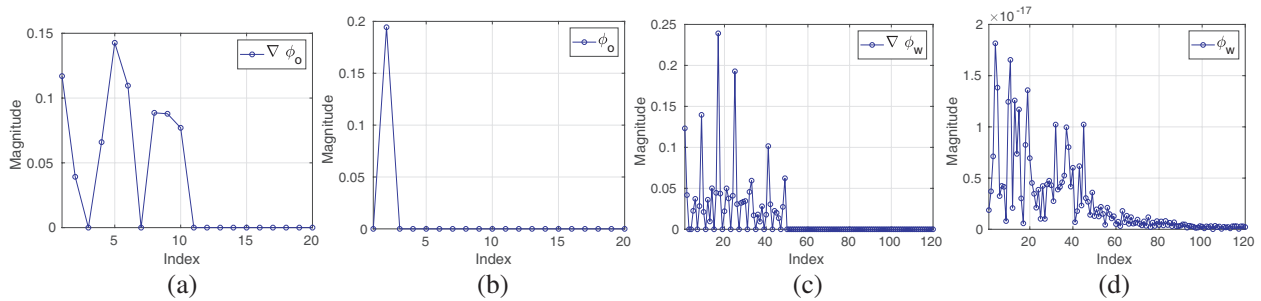


Figure 6: Magnitude of DCT coefficients of estimated tangential fields for 150 measurements. Coefficients corresponding to  $\phi_w$  are almost zero. There are 45 non zero coefficients. (a)  $\nabla\phi_o$ . (b)  $\phi_o$ . (c)  $\nabla\phi_w$ . (d)  $\phi_w$ .

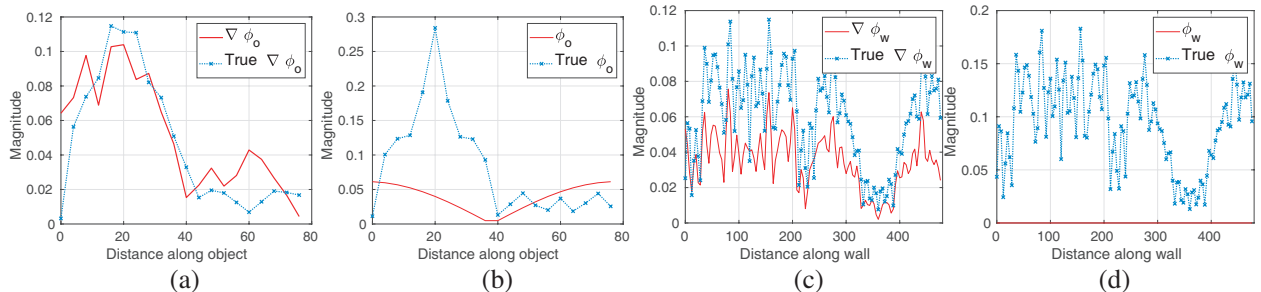


Figure 7: Magnitude of estimated tangential fields using DCT basis for 150 measurements.  $\phi_w$  is almost zero. (a)  $\nabla\phi_o$ . (b)  $\phi_o$ . (c)  $\nabla\phi_w$ . (d)  $\phi_w$ .

reference using the following relation:

$$\text{error} = \frac{\|\phi_{\text{est}} - \phi_{\text{true}}\|_2}{\|\phi_{\text{true}}\|_2}$$

where  $\phi_{\text{est}}$  and  $\phi_{\text{true}}$  are the estimated and true fields over the 2D grid of points respectively. The term sparsity is used to indicate the number of coefficients in the vector that are at least  $10^{-4}\%$  of the maximum value in the vector. The error has been tabulated for all three basis in Table 1.

Table 1: Comparison of reconstruction error and sparsity of the solution in Fourier series, wavelet and DCT basis. The total number of variables are 280.

Measurements	Fourier Series		Wavelet		DCT	
	Error %	Sparsity	Error %	Sparsity	Error %	Sparsity
50	69.36	72	45.41	54	49.51	35
100	30.21	63	24.24	66	18.54	42
150	19.81	65	9.50	70	6.71	45
200	9.56	65	8.09	69	4.91	45
250	8.96	65	6.14	71	4.71	45

#### 4. DISCUSSION

In this work, we have shown that in an indoor scenario, the electromagnetic fields can be reconstructed everywhere in space by making spatial field measurements — to varying levels of error depending on the number of available measurements. For example, we can recover the fields using DCT basis up to less than 10% error using 150 measurements (see Table 1).

An interesting observation is that while the recovered tangential fields on the scatterer surfaces differ significantly from the true fields (see Figures 3, 5 and 7), the fields predicted everywhere based on these tangential fields (using Huygens' principle) agree quite well with the true fields (see Figure 8). This is an artefact of the fact that the matrix equation in our problem is underdetermined and hence admits infinite solutions. It has been verified that the difference between the 'true'

solution and the solution obtained from DCT basis lies in the null space of the system matrix ( $A_p$ ). Due to this, the predictions of the field are still accurate.

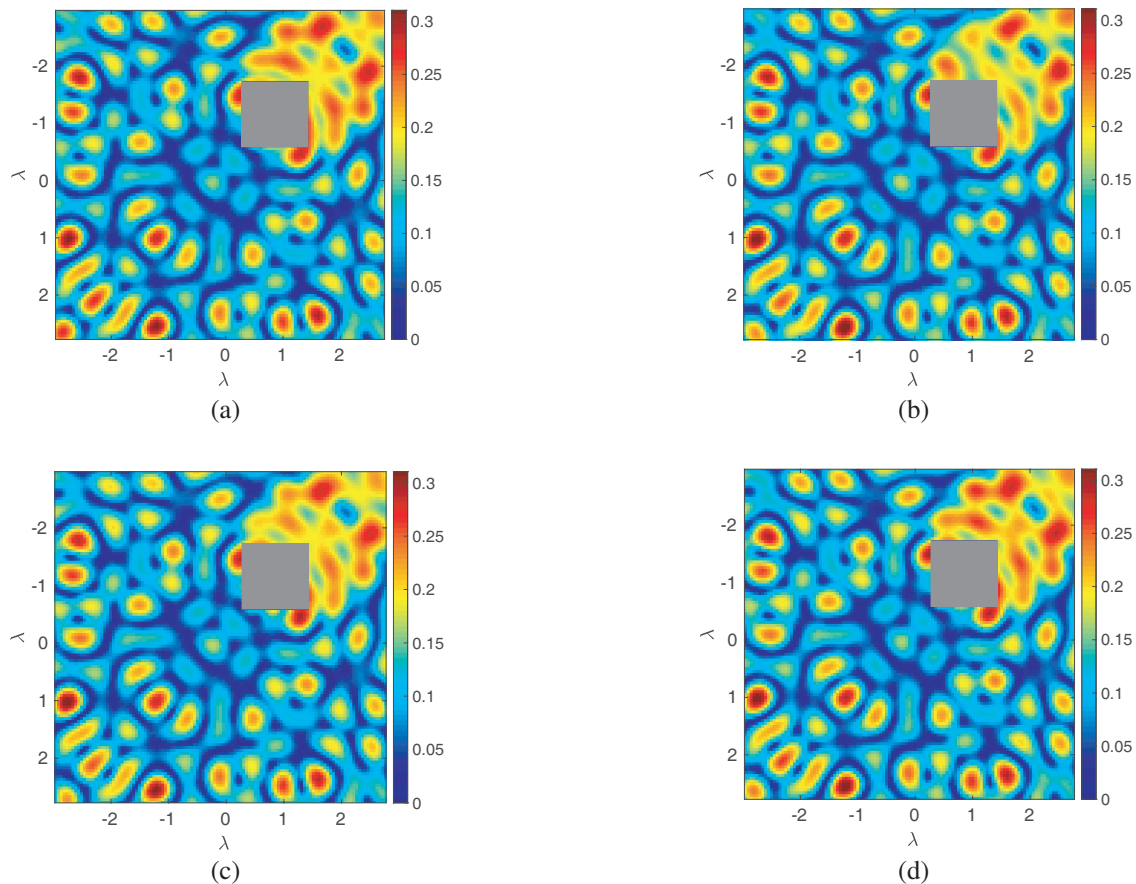


Figure 8: Comparison of reconstructed 2D fields for 150 measurements. (a) Magnitude of true scattered field on a  $6\lambda \times 6\lambda$  grid. (b) Estimated 2D field using Fourier series basis. (c) Estimated 2D field using db2 wavelet basis. (d) Estimated 2D field using DCT basis.

It is also interesting to note that both DCT and Wavelet coefficients are very sparse in  $\phi$ , suggesting that  $\nabla\phi$  is sufficient for reconstruction. Theoretically, this is not surprising, since the Uniqueness theorem requires specification of either the tangential electric *or* magnetic field on entire scatterer surfaces — not both, whereas in the simple formulation of Eq. (1) both fields seem to be required. A similar idea has been leveraged in the so called single integral equation approaches [9, 10].

Among the three sets of basis, we have shown that while Fourier series basis gives a dense solution, DCT and wavelet bases admit more sparse solutions. A quick look at Table 1 will reveal that DCT basis results in the least error, followed by wavelet basis and finally Fourier series basis. So by both criteria (sparsity and error), the DCT basis seems to be the best among the three for this application.

In future work, we will explore the solution of this problem in the presence of amplitude-only data, and also investigate extensions to three dimensions and validation of the algorithm with experimental data.

## REFERENCES

1. Pei, L., R. Chen, J. Liu, H. Kuusniemi, T. Tenhunen, and Y. Chen, “Using inquiry-based Bluetooth RSSI probability distributions for indoor positioning,” *Journal of Global Positioning Systems*, Vol. 9, No. 2, 122–130, 2010.
2. Wu, Z.-H., Y. Han, Y. Chen, and K. J. Ray Liu, “A time-reversal paradigm for indoor positioning system,” *IEEE Transactions on Vehicular Technology*, Vol. 64, No. 4, 1331–1339, 2015.

3. Bose, A. and C. H. Foh, “A practical path loss model for indoor WiFi positioning enhancement,” *2007 6th International Conference on Information, Communications & Signal Processing*, 1–5, IEEE, 2007.
4. Candès, E. J. and M. B. Wakin, “An introduction to compressive sampling [a sensing/sampling paradigm that goes against the common knowledge in data acquisition],” *IEEE Signal Processing Magazine*, Vol. 25, No. 2, 21–30, 2008.
5. Bhat, C., A. Gupta, R. Ganti, and U. K. Khankhoje, “Spatial prediction of electromagnetic fields using few measurements,” *2018 Progress In Electromagnetics Research Symposium (PIERS — Toyama)*, 565–569, Japan, August 1–4, 2018.
6. Chew, W. C., *Waves and Fields in Inhomogeneous Media*, IEEE Press, 1995.
7. Balanis, C. A., *Advanced Engineering Electromagnetics*, John Wiley & Sons, 1999.
8. Candès, E. J., M. B. Wakin, and S. P. Boyd, “Enhancing sparsity by reweighted L1 minimization,” *Journal of Fourier Analysis and Applications*, Vol. 14, Nos. 5–6, 877–905, 2008.
9. Marx, E., “Single integral equation for wave scattering,” *Journal of Mathematical Physics*, Vol. 23, No. 6, 1057–1065, 1982.
10. Yeung, M. S., “Single integral equation for electromagnetic scattering by three-dimensional homogeneous dielectric objects,” *IEEE Transactions on Antennas and Propagation*, Vol. 47, No. 10, 1615–1622, 1999.